Density functional calculations on the intricacies of Moiré patterns on graphite

J. M. Campanera,* G. Savini, I. Suarez-Martinez, and M. I. Heggie
Chemistry Department, University of Sussex, Falmer, Brighton BN1 9QJ, United Kingdom
(Received 14 March 2007; published 28 June 2007)

Scanning tunneling microscopy (STM) imaging has detected a wealth of puzzling features on the surface of highly oriented pyrolytic graphite, among them, anomalously large superperiodicities, called Moiré patterns, caused by the lattice-mismatched top layer of graphite. Exactly, the top graphene layer rotates with respect to the graphite substrate. Such rotation gives rise to different types of local stackings in the different surface graphite regions. As STM mapping is highly dependent on the differences of local density of states of the graphite surface at the Fermi level, variations in brightness differentiate graphite regions with different local stackings. Bright areas (visible graphite areas) correspond to *AABABAB*... local graphite stackings, whereas dark areas (hidden graphite areas) to *BABABAB*... or *CABABAB*... ones. We have programmed an algorithm which first built systematically the whole range of Moiré structures and afterwards quantified the percentages of the different local graphite stackings. Finally, periodic density functional theory calculations have been performed on a selection of Moiré structures in order to draw the energy profile of the rotation between two graphene layers.

DOI: 10.1103/PhysRevB.75.235449 PACS number(s): 68.35.−p, 68.37.Ef, 61.50.Ah

I. INTRODUCTION

The capability of scanning tunneling microscopy[1] (STM) to produce atomically detailed images of surfaces has contributed enormously to the current understanding of surface structures. It has proven to be useful not only in the imaging of defects[2,3] but also in mapping periodic structures.[4] As an example for the first case, STM has been used to reveal the presence of a pentagon at the apex of the protuberance of a graphitic particle.[5] For the second case, highly oriented pyrolytic graphite (HOPG) has become a popular substrate for the STM technique due to its atomically smooth surface and its inert nature.[6,7] Moreover, these atomic resolution images can even be obtained routinely by STM in this substrate in atmospheric, aqueous, and vacuum environments. Nevertheless, literature reports a diverse number of puzzling features in these STM images, among others,[7,8] anomalously large superperiodicities with large atomic corrugations referred to as Moiré patterns.[9] The periodicities of the Moiré patterns are usually several to tens of nanometers.[10,11] STM images can also capture different domains of Moiré patterns delimited by sharp boundaries.[12]

Moiré patterns on HOPG can be induced under a huge range of experimental conditions, but basically they can occur in three main situations: (a) when HOPG is prepared under dry conditions and then immersed in aqueous solutions or in organic solvents like dichloroethane[13,14] or also treated by continuous trials with an adhesive tape in air;[15,16] (b) when metal atoms aredeposited on monolayer graphite[10,17] or HOPG surface;[18] and (c) they are also observed near or along grain boundaries, lattice dislocations, defects, or steps.[12,15,19] The most likely explanation in the first case is based on the intercalation into the interlayer spacing of molecules from solution or solvents making the topmost layer slide.[20] In the second case, rotation and other types of damage seem to be caused by the energy transfer from condensing metal atoms to the substrate.[18] In the third case, the presence of all these discontinuities in graphite seem to clearly stabilize Moiré patterns. It is important to notice that in all cases there are always several domains separated by sharp boundaries, never one domain in isolation.

Hexagonal superstructures are hidden behind these superperiodicities of the Moiré patterns on graphite. Recently, Beyer *et al.* unambiguously showed that the hexagonal superstructures are formed by the mechanical rotation of one top layer with respect to the underlying crystal.[16] However, at the beginning, it was intuitive to interpret STM superlattice structures as corrugations reflecting a physical buckling of the top graphite layer. This fact was disproved by Rong and Kuiper[10] since the interlayer distance between the rotated monolayer and the bulk was measured to be 3.3 Å, as compared with the experimental spacing of 3.35 Å.[21] Thus, the corrugation of a superlattice is unlikely to represent the real atomic arrangement; contrarily, it has been shown that it is highly dependent on the setup (bias voltage and tunneling current) of the STM technique. Finally, Kuwabara *et al.*,[22] Xhie *et al.*,[23] and Rong and Kuiper[10,15] also provided convincing arguments in support of the explanation that superlattices are Moiré patterns resulting from rotational misorientation of graphite layers, such as the matching of experimental rotation angles with theoretical ones under the assumption of the Moiré pattern hypothesis.

HOPG consists of layers of sp^2 carbon atoms, weakly bonded together by van der Waals forces into a *BA*-stacked sequence along the z axis.[24] This stacked sequence gives rise to two inequivalent carbon sites in the surface: α-site carbon atoms lie directly above a second layer atom, whereas the β-site carbon atoms are located above the center of the sixfold carbon ring in the second layer.[25,26] STM mapping is highly dependent on the local density of states (LDOS) at the Fermi level of the sample surface.[27] Calculations revealed strong asymmetry of LDOS between the two sites of carbon atoms in the top graphene layer.[25] β-site carbon atoms are much easier to detect by STM since these atoms have a higher LDOS near the Fermi level. In other words, β-site carbon atoms are the only visible (bright) atoms in STM images, whereas α-site carbon atoms remain invisible or hid-

den (dark). Since α- and β-site carbon atoms are equally distributed on the hexagonal lattice, 3 out of 6 atoms of the regular graphene hexagon are invisible. So, these β-site carbon atoms form a new larger hexagonal structure, i.e., triangular structure. This phenomenon explains why the regular graphene honeycomb structure with all six carbon atoms is rarely observed, except under certain unusual experimental conditions.[28,29]

The correspondence between structure and intensity of STM has also been studied in depth in Moiré patterns on graphite. Unfortunately, a common model has not emerged yet as a recent review shows.[30] The structural purity seen in *BA* graphite is broken in the Moiré structures, and consequently, the division between α- and β-site carbon atoms becomes meaningless. Instead of classification through single carbon atoms, one argues on the local stacking of the graphite regions created after the rotation. Hence, a clear correlation between the local stacking, LDOS of the graphite surfaces at the Fermi level, and the STM images is necessary in order to understand the phenomenon. Two models have been proposed. Each invokes a different correlation between structure in the local regions and brightness in the STM images. The model[23] of Xhie *et al.* is based on the assumptions of the STM of *BA* graphite, whereas Rong and Kuiper's model[10] relies on *ab initio* calculations of the density of states (DOS) of perfect *AA*-, *BA*-, and *CAB*-stacked graphites. This discussion will be extended below.

The purpose of this study is to obtain a comprehensive picture of the Moiré patterns on graphite from the theoretical point of view and, finally, clarify the controversies around the correlation between local graphite stacking and brightness in STM images. In order to accomplish this, we performed the following steps: first, DOS was calculated for several reference structures in order to fully understand STM images; second, a program to generate the whole range of Moiré structures was created; third, some experimental Moiré patterns images were theoretically simulated by means of a simple two graphene layer superposition model; fourth, each generated structure was topologically characterized by quantifying the percentage of the different types of local graphite stackings; and finally, selected structures were geometrically optimized by means of density functional theory (DFT) periodic calculations and the energy profile of the rotation process was obtained.

II. COMPUTATIONAL DETAILS

Ab initio calculations have been performed on selected Moiré structures within DFT using the AIMPRO package.[31] The exchange-correlation energy has been determined using the local density approximation, with the functional as parametrized by Perdew and Wang.[32] The employed wave function basis sets consist of *s*, *p*, and *d* Gaussian orbital functions, with four exponents centered at the atomic sites.[31] Norm-conserving pseudopotentials based on the Hartwigsen-Goedecker-Hutter scheme are used,[33] while the charge density is expanded in plane waves up to 300 Ry. The numerical integration over the Brillouin zone is performed using the Monkhorst-Pack special *k*-point technique.[34] The size of the *k*-point mesh is chosen so that the average density of the *k* points for all computed structures would approximately correspond to that of a $19\times19\times7$ mesh in the four-atom hexagonal unit cell describing the *BA*-stacked graphite. We used the supercell approach with periodic boundary conditions. The lattice parameters for *BA*-stacked graphite are excellent ($a=2.452$ Å and $c=6.642$ Å, compared with experimental $a=2.461$ Å and $c=6.709$ Å).[35] Furthermore, the DOSs have been calculated for several reference structures. In this case, the sampling grid had to be increased considerably, up to $63\times63\times23$, in order to get converged values.

III. RESULTS AND DISCUSSION

A. Local stacking, density of states, and scanning tunneling microscopy

Visible areas in STM are represented by bright points, whereas invisible areas by gray and/or dark ones.[36,37] Graphite STM images on Moiré patterns show bright areas in a centered-hexagonal lattice, each surrounded by a hexagonal ring of six gray and/or dark valleys. At this point, it is crucial to assign a structure to each area of different intensity of the STM image. Two models have been presented so far. Xhie *et al.*[23] have distinguished three different regions in the topmost layer in a location relative to the *BA*-stacked substrate. An atom in the top layer can be above any site in the second layer, an α site, a β site, or a hole site, or anywhere in between these locations. In an M-h-site (in the nomenclature of Xhie *et al.*), atoms in the top layer are either covering an α site or a β site in the second layer. In an M-α-site (M-β-site), atoms in the top layer are either above hole sites in the second layer or above β sites (α sites). Although not proven by theoretical calculations, but instead, by what one could expect from the analogy from the assignation made for perfect *BA*-stacked graphite, Xhie *et al.* did the assignation as follows: the M-h-sites correspond to the darkest areas in STM superlattice images, whereas the M-β-sites correspond to the brightest areas and the M-α-sites to the second brightest ones.

On the other hand, Rong and Kuiper[10] identified four kinds of areas with local stacking orders (hereafter named, according to their structural resemblance to the perfect structures with this nomenclature): *AAB* (brightest), *CAB* (darkest), Slip*BAB* (second brightest), and *BAB* (second darkest). In that case, the assignation was made on the basis of (1) the relative corrugation of the different areas in STM images and, most importantly, (2) the band-structure calculations that revealed, strikingly, that the DOS at the Fermi level of simple hexagonal *AA*-stacked graphite is about three times higher than that of rhombohedral *CAB*-stacked or normal hexagonal *BA*-stacked graphite.[38,39] The controversy comes from the fact that M-β-sites (brightest) in the model of Xhie *et al.* correspond to *BAB* (second darkest) in Rong and Kuipers model, and furthermore, the M-hole-sites (darkest) correspond to *AAB* (brightest).

So, the model of Xhie *et al.* and the model of Rong and Kuiper use different ways to explain the correlation between local stackings and DOS, arriving at different conclusions. To solve the controversy, we computed the DOS at the Fermi

level for the following stackings: *AABABAB*, *BABABAB*, Slip*BABABAB*, and *CABABAB*, which resembles the situation where the first layer is rotated in relation to *BA* bulk graphite. Additionally, an extra 5 Å vacuum space is added between the two layers of different unit cells with the purpose of simulating a surface. The computed DOSs at the Fermi level are 0.0046, 0.0037, 0.0042, and 0.0038 states/eV atom, respectively.[40] Therefore, our findings confirm Rong and Kuiper's model. So, *AAB*-stacked graphite areas appear to protrude in the STM images, and therefore, they form the bright spots in a hexagonal lattice fashion. On the other hand, the dark areas consist of almost indistinguishable *BAB*- and *CAB*-stacked graphite.[41] Finally, the Slip*BAB* represents an intermediate bright intensity. For completion purposes, the DOS spectrum of each of these reference structures is plotted in Fig. 1. The different DOS spectra appear to be rather similar to the pure *BABABAB*-stacked graphite across the whole range of energies, except in the specific regions around −2.5 eV [Fig. 1(b)] and 1.5 eV [Fig. 1(c)]. The general features of the surface model *BABABAB*-stacked graphite coincide with those features already reported for bulk *BA* graphite.[42]

B. Obtaining Moiré structures

Our starting structure for creating Moiré patterns on graphite is the most stable graphite structure, *BA*-stacked graphite. As a first approximation, the unit cell is formed only by two layers of carbon atoms without extra vacuum space in the z direction, called hereafter the bulk model. Depending on the two different rotation centers (β- and α-site carbon atoms), different rotation pathways can be created, each leading to different groups of structures. However, both pathways share the same angle range, from 0° to 60°, due to the D_{6h} symmetry of the crystal according to Bernal type classification.[43] In the first case, a rotation from a β-site carbon atom as a rotation center will lead, after 60°, again to the same starting material: perfect *BA*-stacked graphite; hereafter called the β bulk model. Contrarily, an α-site carbon atom as a rotation center will lead to a perfect *AA*-stacked graphite, called analogously the α bulk model. Furthermore, a careful inspection reveals that 30° rotation represents a symmetry point, and that only the 0°–30° angle range need to be studied.[44]

With the aim to ratify the results, a larger model has also been built. Unlike the previous model, we used four layers of *BA*-stacked graphite and only the top one was allowed to rotate from a β-site carbon atom as a rotation center. Moreover, an extra 5 Å vacuum between unit cells in the z direction was added. This model was named β surface model and represents a more reasonable approach to the reality of this surface phenomenon, in which only the topmost layer rotates in relation to the *BA* graphite substrate. More geometrical details of the models in regard to the energy calculations will be given in the last section.

Despite two different models, it is important to notice that Moiré patterns on graphite decay rapidly through the z direction and, moreover, it is very unlikely that a Moiré contrast several layers below can be detected by the STM technique,

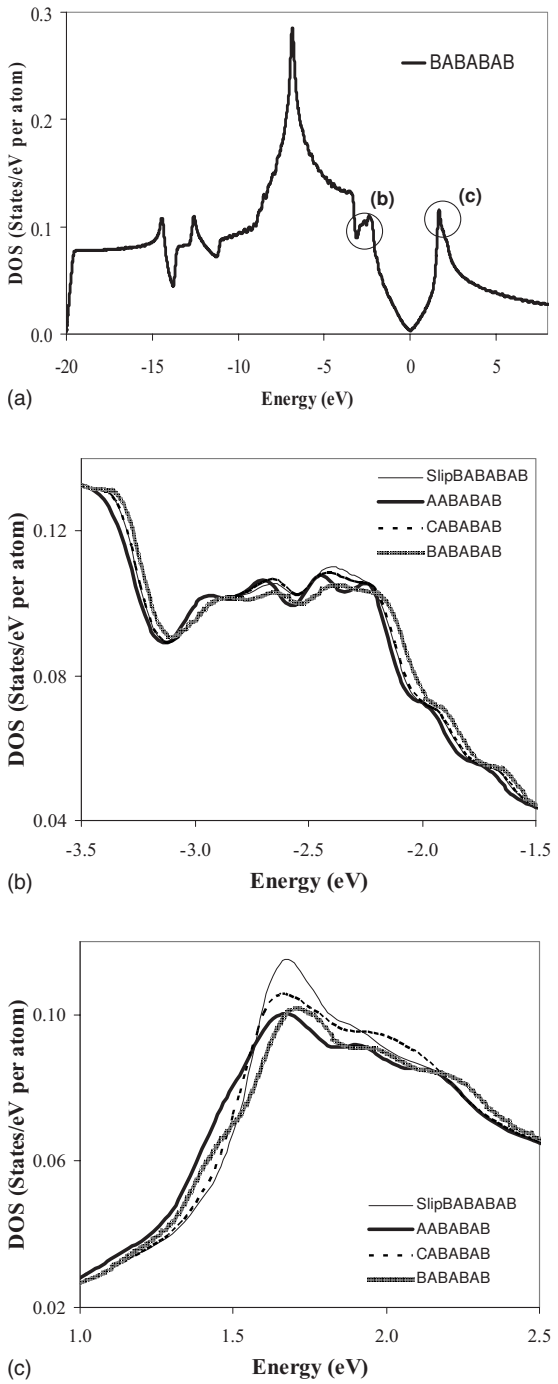

FIG. 1. DOS plot for the reference surface graphite structures. (a) Since all DOS spectra are almost identical, only the DOS for the surface model *BABABAB*-stacked graphite has been plotted for the full range of energies. (a) The densities of states for the remaining reference structures (*AABABAB*, Slip*BABABAB*, and *CABABAB*) are plotted in those regions where they are different: (b) around −2.0 eV and (c) 1.5 eV. The Fermi level is centered at the origins of the graphs.

since this is sensitive to LDOS variation on the surface basically.[27,45] In consequence, it is expected that the bulk model that simulates only two monolayers of graphite should be enough to fairly reproduce the physical phenomenon. More advanced models could be built to simulate Moiré pat-

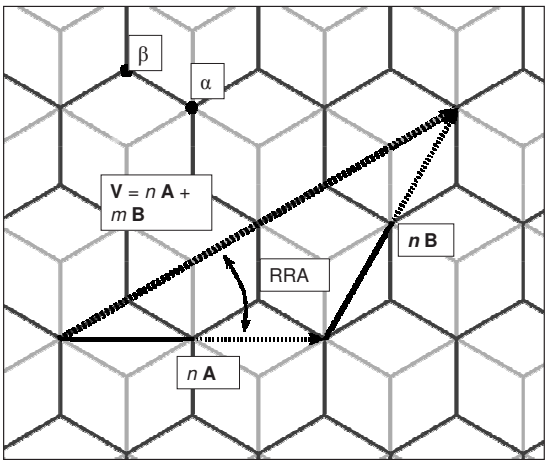

FIG. 2. Representation of the relative rotation angle (RRA) as the angle between **A** vector and the vector sum of n**A** and m**B** vectors (**V**), where **A** and **B** are graphene vectors, and n and m are integers. So, $\mathbf{V}=n\mathbf{A}+m\mathbf{B}$. In the particular case shown above, n and m are set to 2, thus, RRA=60°. If one applies that rotation, the topmost layer (black lattice) rotates 60° in relation to the bottom one (gray lattice). α- and β-site carbon atoms are also drawn. Observe that the rotational center is an α carbon atom and the starting material is perfect *BA*-stacked graphite.

terns on graphite. For example, these advanced models would bring light to the subtle region, where perfect *BA* graphite upon an infinitesimal rotation dramatically changes to a Moiré structure.

If one looks at the possible orientations of two rotated layers in detail, some special orientations are found. The Moiré structures develop, for certain angles, some coincidence site lattice (CSL) points.[46] Some lattice sites of the topmost layer coincide exactly with some of the lattice sites of the underlying layer. Obviously, it is important to remark that one is not simply looking for coinciding atom positions but, rather, for coinciding lattice points in the crystal. This principle has been used to build up systematically the whole range of Moiré structures on graphite. Hence, instead of the relative rotation angle (RRA) between two graphite layers to be chosen, a selected angle is made in order to get a unit cell with a CSL. A CSL is obtained after the first layer is rotated over the second one according to the RRA between the n**A** and **V** vectors. The **V** vector is the vector sum of n**A** and m**B** vectors, $\mathbf{V}=n\mathbf{A}+m\mathbf{B}$. (n,m) are the vector components and $(\mathbf{A},\mathbf{B})$ are vectors of the graphene lattice. All vectors and the RRA are represented in Fig. 2. The full variation of the n and m components will allow us to obtain a complete range of structures with different RRAs. High integer values of the n and m components produce small RRAs between both graphene layers. A FORTRAN program that varies both n and m from 1 to 30 (with the constraint that $n>m$) was created for that purpose. For each of the three models, 426 different Moiré structures were constructed with RRAs ranging from 1.12° to 29.96°.

Figure 3 graphs the number of atoms per unit cell for the Moiré structures depending on their RRAs. As can be seen, the FORTRAN program generates a large number of structures with a strongly varied number of atoms per unit cell. Notice

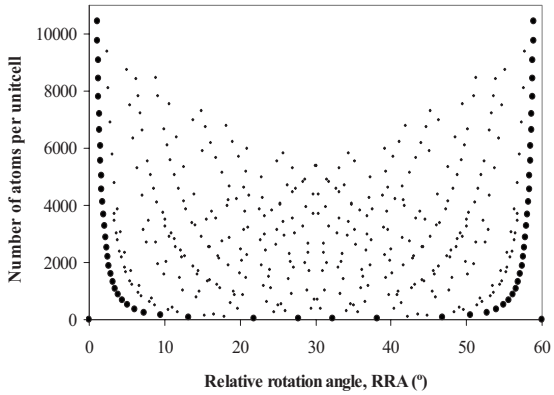

FIG. 3. Number of atoms per unit cell for the β bulk model. The starting and final graphite structures are perfect *BA*-stacked graphite (0° and 60°). Bold dots are the smallest unit cells possible, the rest, quasiunit cells. Notice the symmetry of the graph about 30°.

that similar Moiré structures—structures with slightly different RRA—can be reconstructed by a formidable range of unit cells with different number of atoms in each of them. In other words, unit cells with different numbers of atoms can produce similar Moiré structures. Structures which are formed by a huge number of atoms per unit cell and, additionally, for which a slight change to their RRAs leads to a structure with a few atoms per unit cell exhibit quasiunit cells. For instance, a 21.8° RRA structure is obtained with (n,m) components of (2,1) and only 28 atoms are needed to represent it, whereas the relatively close structure of 22.5° RRA needs more than 10 000 atoms to be represented with the (39,19) components in the FORTRAN algorithm. The issue is that the Moiré pattern need not have exact translational symmetry compatible with the lattice vectors of the underlying lattice—its periodicity does not rely on strict translation symmetry in atom positions. The periodicity in the pattern can be much smaller than the formal periodicity of the twist boundary unit cell.

According to the Moiré pattern hypothesis, mathematically, the periodicity of a Moiré pattern (D) arising from a RRA between hexagonal lattices is $D=d/[2\sin(\mathrm{RRA}/2)]$, where $d=2.452$ Å is the basal lattice constant of graphite.[13,47] In the present paper, all periodicities are referred to this last definition, periodicity of the Moiré patterns, unless otherwise stated. As the angle of misalignment decreases, the superlattice periodicity of the Moiré pattern increases. This can be corroborated in all experimental STM images. Figure 4 plots this relationship for the β bulk model. Observe that the minimum periodicity of 4.75 Å is obtained at 30° RRA, and on the other hand, there is no maximum as the function tends to infinity in the vicinity of 0° and 60° RRA. Thus, 0° and 60° RRA are discontinuity points. These transitional areas between perfect *BA*-stacked graphite and Moiré structures at extremes of the plot suggest great changes when the rotation process starts.

C. Simulation of Moiré pattern images

The simulation of Moiré pattern images on graphite and its comparison with experimental ones help us to confirm the

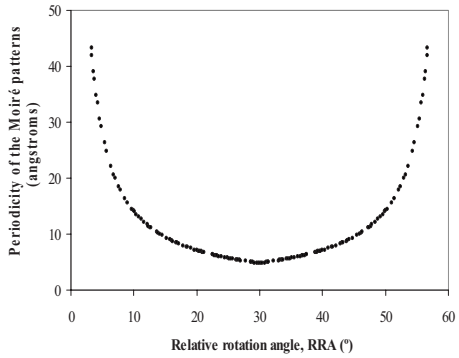

FIG. 4. Periodicity of Moiré structures, D. RRA and D are related as $D=d/[2\sin(\mathrm{RRA}/2)]$, where $d=2.452$ Å is the lattice constant of graphite. That mathematical relation came from the Moiré pattern hypothesis that when two structures are rotated, the resulting interfering periodic lattices cause a superperiodic structure having the same symmetry as the original lattice. Moiré patterns are interference patterns that can arise from rotation between two layers of any repeating lattice. Notice the symmetry of the graph about 30°.

hypothesis underlying the Moiré pattern theory. The correlation between atomic structures and local densities of states of carbon structures has been directly verified by STM.[3,48] STM simultaneously provides information about atomic structures and electronic states of surfaces with atomic resolution.[45] Therefore, a reasonable simulation of STM images would be a reconstruction of the local density of states at the surface level.[45,49] So, obviously, Moiré pattern images on graphite could be reproduced by means of theoretical STM reconstruction but accompanied with a considerable computational effort. Instead, in our case, a more rudimentary, but effective, methodology has been implemented, consisting of images of superimposed structures. This methodology has already been used by Cee *et al.*[13] As we argued above, the brightest areas in STM images represent *AAB*-stacked graphite, while dark and gray areas represent *BAB* or *CAB* and Slip*BAB*, respectively, as stated by Rong and Kuiper. However, as our model only contemplates two graphene layers, the whole picture is slightly simplified: *BAB* and *CAB* local graphite stackings are no longer differentiated in a two-layer model and they become identical. So, in our model, *AA* stacking is represented by the brightest areas, *BA* stacking by the darkest and gray areas, whereas Slip*BA* by the second brightest areas. These types of local graphite stackings are depicted more clearly in the plot of Fig. 5. Actually, the atomic superposition of two graphene layers, one rotated against the other, reproduces the same visual effect.

To prove that, an STM image of graphite showing a Moiré pattern of approximately 1.28° of RRA and 110 Å of periodicity from Ref. 28 has been reproduced satisfactorily (see Fig. 6).[50] We chose the closest structure from the β bulk model to the experimental one: 1.30° RRA structure with 109 Å periodicity. The reconstructed Moiré pattern image in Fig. 6(b) shows only a superimposed vision of the stick model of the two graphene layers. The simple model succeeds in reproducing the essential characteristics of the experimental STM image: (a) the brightest areas correspond to *AA*-stacked graphite because there is free space left, since

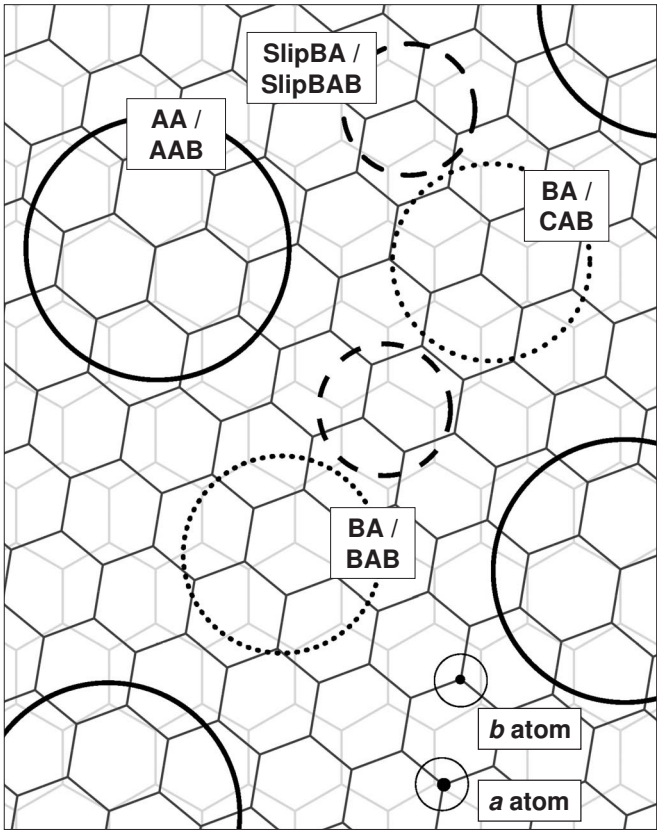

FIG. 5. Different local graphite stackings with two and three graphene layer models that reproduce those stackings found in Moiré patterns. Three graphene layer model from Rong and Kuiper: *AAB*, *BAB*, *CAB*, and Slip*BAB*. Two graphene layer model: *AA*, *BA*, and Slip*BA*. If three graphene layers are taken into account, then the *BA* stacking gets separated into *BAB* and *CAB* local stackings, whereas the rest remains the same: *AA* is named *AAB* and Slip*BA* is now named Slip*BAB*. The threshold value (δ)—radius of the small circumferences—was used to distinguish between *a* and *b* carbon atoms in the algorithm that classifies local graphite stackings into *AA*-, *BA*-, and Slip*BA*-stacked regions when two graphene layers are used. The positions of all carbon atoms of one layer are projected onto the other layer, and as a result, some carbon atoms (*a* atoms) have one neighbor within a lower distance than an arbitrary threshold value (δ) and some do not (*b* atoms).

top and bottom atoms coincide; (b) the darkest and gray areas (just in the central area between three bright areas) correspond to the *BA*-stacked graphite; and, finally, (c) the second brightest areas between two close bright areas correspond to the Slip*BA*-stacked graphite. Notice that the pattern and number of the brightest areas along the x and y directions coincide for the experimental and simulated images. Look carefully that there are two intensities of dark (*BAB* and *CAB*) in the experimental image but only one dark area (*BA*) in the simulated one. The structure with 1.30° RRA was built with (26,25) components in the FORTRAN algorithm and it possesses 7804 atoms in its unit cell, although to build such 50×50 nm^2 image, more than 200 000 atoms were required by repeating the unit cell along the x and y axes.

Figure 7 shows simulated Moiré pattern images on graphite aiming to cover the whole range of RRAs (5.1°, 7.3°,

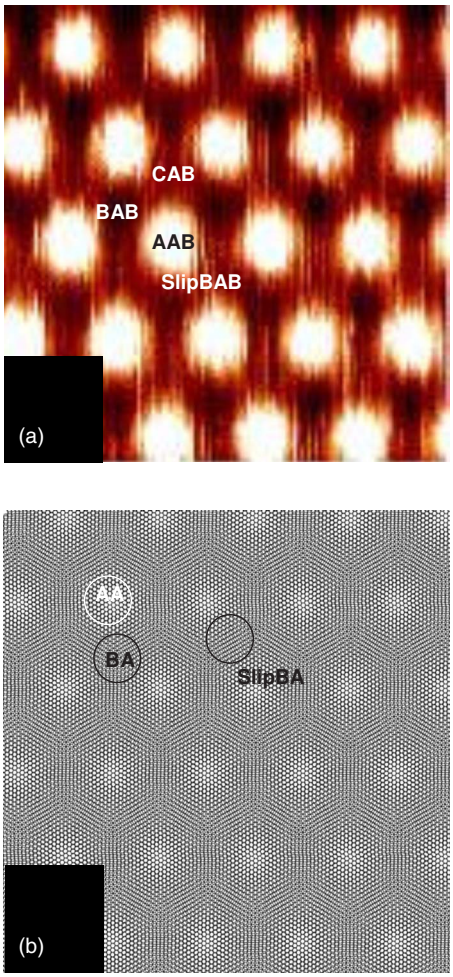

FIG. 6. (Color online) Molecular image that reproduces a STM Moiré pattern image. (a) Experimental STM Moiré image of 1.28° RRA and 11.0 nm of periodicity. Reprinted from Fig. 3(c) of Ref. 28. (b) Molecular image that simulates a Moiré pattern of 1.28° RRAs and of 10.9 nm periodicity. The molecular image is taken from the β bulk model with (26,25) components in the algorithm. The molecular image is built according to the superimposition vision of a stick model of two graphene layers. The different local graphite stackings (*AAB*, *BAB*, *CAB*, and Slip*BAB*) in a Moiré pattern are located in the experimental image. Analogously, it is also done (*AA*, *BA*, and Slip*BA*) in the two layer model that simulates the Moiré pattern. More details on these structures are drawn in Fig. 5. Scanning areas $\sim 50 \times 50$ nm^2.

13.1°, 16.4°, 21.8°, and 27.8°) and also to exhibit all interesting patterns created by this phenomenon. These images approximately represent a 10×10 nm^2 scanning area and are built from the β bulk model structures. Looking carefully at the first plot (5.1° RRA), one can visually distinguish the two kinds of regions with high rotation symmetry we mentioned above: *AA*-stacked graphite (bright areas) and *BA*-stacked graphite (dark areas between three close bright areas). Several observations arise from the set of images: (a) the visual Moiré patterns—the coexistence of different contrast regions—almost disappear for the last three pictures (angles more than 15° RRA, approximately), so hereafter, Moiré structures refer to rotation structures with $0° < \text{RRA} < 15°$ only; (b) the smaller the RRA, the bigger the periodicity and the more obvious a Moiré pattern is; (c) the percentage of bright areas decreases from high proportions at small RRAs to almost being wiped out at RRAs around 30°; and (d) as the RRA decreases to 0°, bright regions move farther apart from each other and become larger. Thus, it seems that the quantification of the different types of local graphite stackings and their variation with the RRA between both graphene layers will play an important role in determining the energy profile and unveiling the causes of the formation of such patterns.

D. Quantification of the local graphite stackings

A step forward in the analysis of the Moiré patterns on graphite is not only to visually distinguish the three types of local graphite stackings but also to quantify them formally. A complementary FORTRAN algorithm was programmed to calculate these percentages. The algorithm works as follows. First, all carbon atoms of the top layer are projected onto the bottom layer, then all C-C distances are computed, and the carbon atoms of the former top layer classified into two groups, *a* and *b* atoms. *a* atoms have carbon neighbors at a distance lower than a predetermined threshold value, δ, whereas *b* atoms do not (see Fig. 5 for clarification). Carbon atoms that belong to the *AA*-stacked graphite region turn out to be the easiest to be labeled. Within a layer, an atom is classified to belong to the *AA*-stacked graphite region only if it is labeled as an *a* atom, and all its three in-plane neighbors are also labeled as *a*. On the other hand, the *BA*-stacked graphite region is also determined by means of this rudimentary algorithm. Carbon atoms that belong to the *BA*-stacked graphite region are those which either (a) are labeled as *b* atoms and, moreover, at least two out of its three neighbors are labeled as *a*, or (b) are labeled as *a* and, moreover, at least two out of its three neighbors are labeled as *b*. The remaining atoms that do not belong to either *AA*-stacked or *BA*-stacked graphite regions are classified, consequently, as Slip*BA*-stacked graphite region. Although it emerges from the previous description that the threshold δ plays a key role in this formal classification, we will see that different thresholds will point to the same direction. We are aware that this algorithm does not represent a unique solution to classify the different types of graphite stackings, but it emerges from the analysis that such an algorithm will always imply some arbitrariness to distinguish which is *AA*, *BA*, or Slip*BA*, as we have done.[51]

Figures 8(a) and 8(b) present the stacked profile—percentage of types of local graphite stackings—for the β bulk model with $\delta = 0.7$ and 0.5 Å, respectively. Although they look completely different, both charts provide the same information. The following statements can be extracted from Fig. 8(a), $\delta = 0.7$ Å. Notice, first, that the graph is symmetric around 30° RRA, so, for example, 0° is equivalent to 60° and 15° to 45°. Thus, the discussion will be made in terms of the first half but referring to the whole range. Second, 0° RRA represents a discontinuity point since, even though one approaches infinitesimally close to 0°, the three lines (% *AA*, *BA*, and Slip*BA*) do not tend to the perfect *BA*-stacked

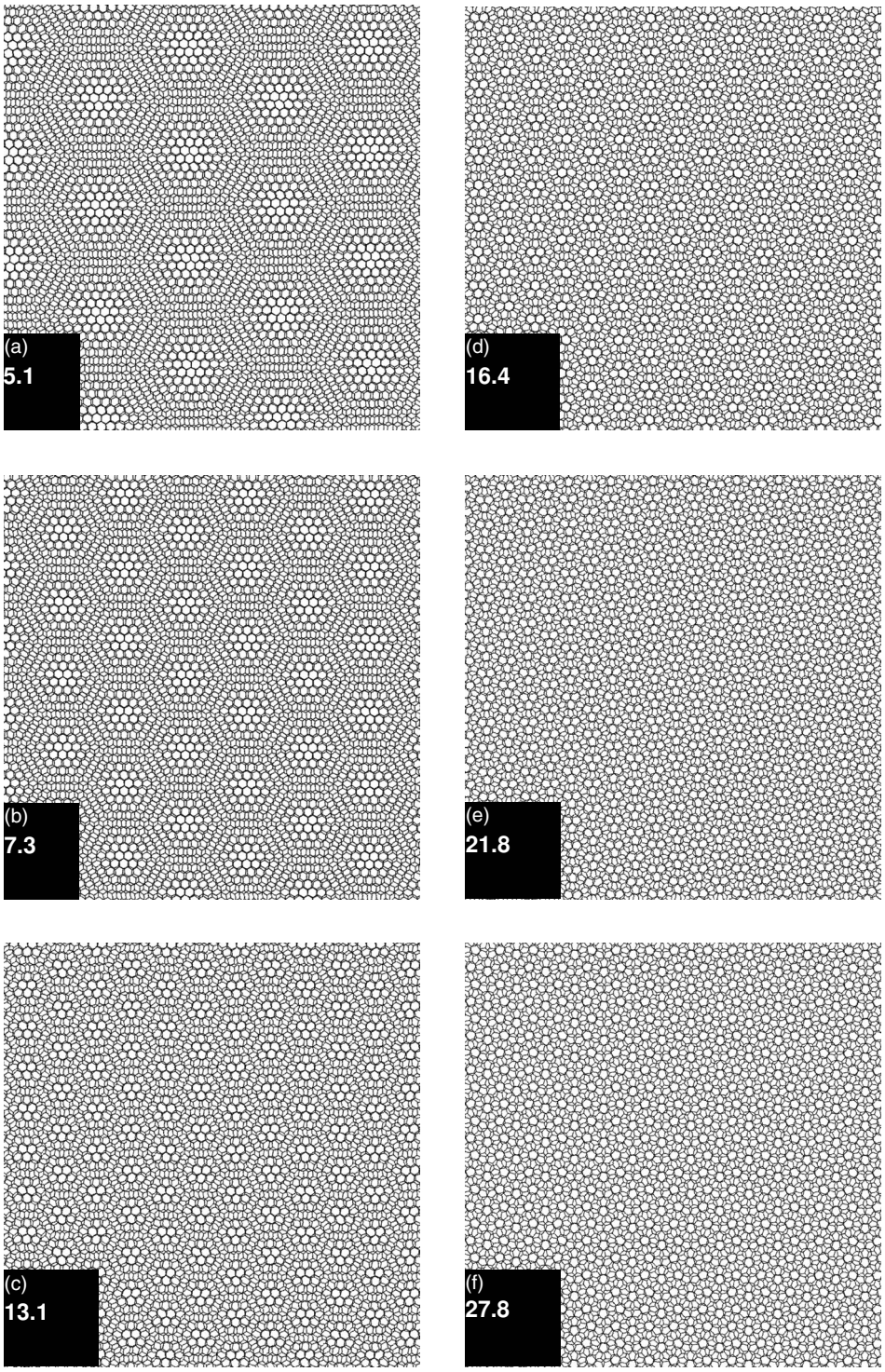

FIG. 7. Molecular images of various rotation structures with (a) 5.1°, (b) 7.3°, (c) 13.1°, (d) 16.4°, (e) 21.8°, and (f) 27.8° RRAs. The periodicities of the patterns (D) are 27.7, 19.2, 10.7, 8.6, 6.5, and 5.1 Å, respectively. Molecular images are built according to the superimposition vision of a stick model of two graphene layers. Rotation structures are taken from the β bulk model. 0° and 60° represent perfect graphite with *BA* stacking. Only the first three plots show Moiré pattern. Scanning areas $\sim 11.0 \times 11.0$ nm^2.

graphite values (% $AA=0$,% $BA=100$, and % Slip$BA=0$). That behavior is nothing new; we argued in the same direction in Fig. 4. Third, the percentage of *AA*- (bright areas) and *BA*-stacked (dark) graphite regions decreases when rotation progresses from 0° to 30° RRA, until these types of local graphite stackings get extinguished around 30°. Simultaneously, the Slip*BA*-stacked graphite region (second brightest) becomes the most common one for the rotation structures around 30° RRA.[52] Fourth, 15° RRA turns out to be a crucial angle which distinguishes the two different groups of rotation structures clearly: those with Moiré patterns and those without. At 15°, the percentage of Slip*BA*-stacked graphite region overcomes first the percentages of *AA*-stacked graphite regions and then those of the *BA*-stacked graphite regions. In other words, there will be more gray areas than bright or completely dark ones. With certain analogies, all these four statements emerge equally clear from the analysis of Fig. 8(b), $\delta=0.5$ Å.

These features are in good agreement with the experimental information provided.[37] One might have expected that

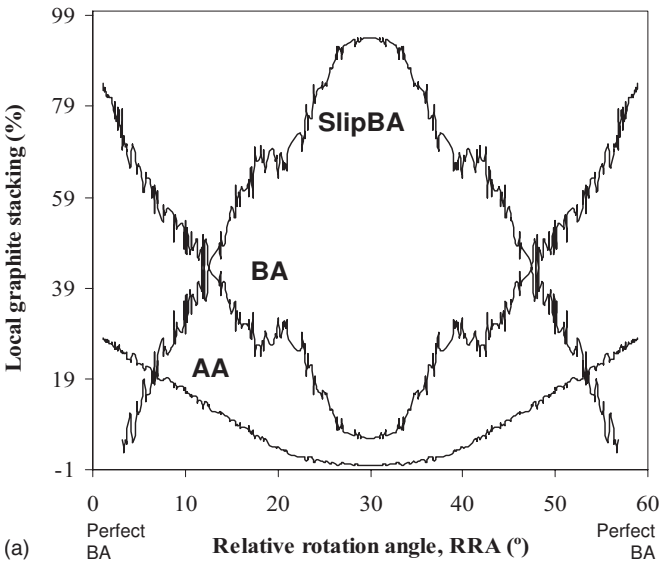

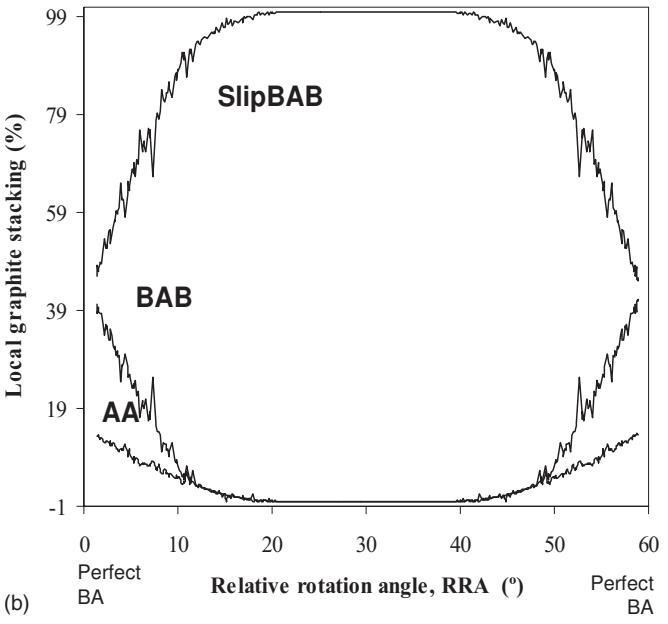

FIG. 8. Percentage of local graphite stackings (*AA*, *BA*, and Slip*BA*) for the structures of the β bulk model: (a) δ=0.7 Å and (b) δ=0.5 Å. The starting and final graphite structures are perfect *BA*-stacked graphite (0° and 60°). Notice the symmetry of the graph about 30°.

such a profile is unique to the β bulk model, but, fortunately, it is not. Figure 9 presents the stacked profile for the α bulk model with δ=0.7 Å, and it provides the same pattern. Therefore, it is confirmed that the starting material (i.e., center of rotation) does not affect the Moiré patterns on graphite, as was also envisaged from experimental data. Experimentalists create STM images and they can even calculate the RRA from the periodicity shown by the image, but they do not control how the first layer rotated, i.e., about which rotational center it did. To sum up, regardless of the rotational center, all simulated images with similar RRA show the same Moiré pattern features.

How do we relate this quantification to the STM images? First of all, it should be noticed that Moiré patterns on graphite only appear approximately within the range: $0° < \text{RRAs} < 15°$. Hence, the rotation structures within the 15°–30° RRA range do not produce any Moiré pattern sufficiently strong to be detected by STM. This rough division at 15° does not pretend to be strict, but merely indicative. Those rotation structures that show Moiré patterns will possess a minimum of approximately 10 Å of periodicity up to several hundreds of angstroms. So, it is not surprising that experimental STM groups report only hexagonal superlattices with periodicities from 17 to 300 Å, never much smaller.[9] In addition, Moiré structures are characterized as having a higher percentage of *AA*- and *BA*-stacked graphite regions than Slip*BA*-stacked one. This situation is reversed in the rotation structures that do not show such patterns. An alternative reasoning is that Moiré patterns on graphite have a high percentage of visible or bright graphite areas. One can easily argue that structures without such patterns do not have a high enough proportion of *AA*- or *BA*-stacked graphite regions and, consequently, all carbon atoms turn out to be indistinguishable by STM, since Slip*BA*-stacked graphite regions become predominant. In other words, the STM technique and its ability to plot the LDOS of the surface can no longer efficiently differentiate the small differences in LDOS among the slightly different carbon atoms in Slip*BA*-stacked graphite. The result is just a grayish image with no bright spots, only tonalities of gray with scant information.

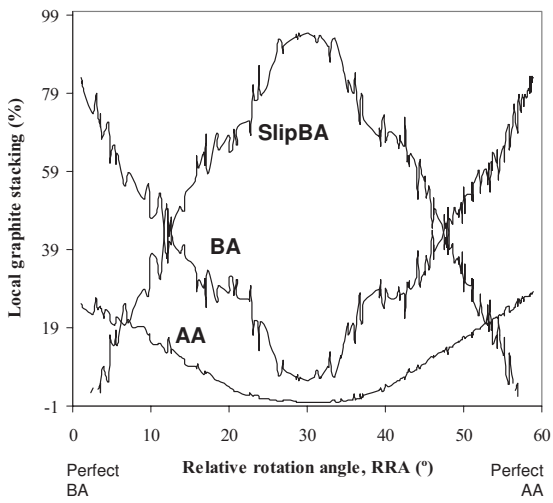

FIG. 9. Percentage of local graphite stackings (*AA*, *BA*, and Slip*BA*) for the structures of the α bulk model. 0.7 Å is set as the threshold (δ) in the algorithm. The starting graphite structure (0°) is perfect *BA*-stacked graphite, whereas the final one (60°) is perfect *AA*-stacked graphite. Notice carefully that the symmetry around 30° has been broken slightly.

E. Energy profile and interlayer separation

Finally, the geometries of all structures with fewer than 500 atoms/unit cell were fully optimized by means of DFT procedures. Fortunately, structures representing all ranges of RRAs were available to be calculated. The interlayer separation and also the intralayer C–C bond lengths were fully optimized for both α and β bulk models. The procedure gave

reasonably precise values for the interlayer separation of perfect *BA*-stacked graphite of 3.321 Å, which compares well with the experimental value of 3.35 Å.[21] The analogous distance for the hypothetical *AA*-stacked graphite is computed to be 3.591 Å, a value that is significantly larger than its counterpart in *BA* graphite. Charlier *et al.* have reported a similar value of 3.66 Å,[53] but others have calculated it to be up to 4.0 Å.[54] Actually, for the interlayer separation of the rotation structures, six distances were tested from the *BA*-stacked graphite interlayer distance (3.321 Å) to that in *AA*-stacked graphite (3.591 Å). They were thus 3.321, 3.375, 3.429, 3.483, 3.537, and 3.591 Å.[55] Regarding the intralayer C–C bond lengths in *BA*-stacked graphite, these were calculated to be 1.418 Å, in good agreement with the experimental value of 1.42.[56] Unlike intralayer C-C distances, interlayer separations vary strongly between both types of graphite structures and are, therefore, important parameters of the Moiré structures. The β surface model was more sophisticated: a set of four layers separated by 5 Å vacuum. In the three bottom layers, the interlayer separation and intralayer C-C distances were taken from those of perfect *BA*-stacked graphite, thus, 3.321 and 1.418 Å, respectively; whereas the interlayer separation of the two top layers was taken from those distances already calculated for the β bulk model. All atom positions within the cell were then allowed to relax with conjugate gradient. Note that this method does not efficiently relax the prismatic direction, so interlayer distances remained at the imposed values.

Table I lists the relative formation energies and characteristics of all calculated structures for the β and α bulk models, the β surface model, and the reference *BA*-, *AA*-, *BABA*-, *AABA*-, *BABABA*-, and *AABABA*-stacked graphite structures. Complementarily, the energy profiles of the two first models are plotted in Figs. 10 and 11, respectively. Our methodology reproduces the energy difference between the perfect *AA*- and *BA*-stacked graphites of 12–14 meV/atom at the two topmost layers,[54,57] calculated here to be 10.3 meV/atom in favor of the *BA*-stacked graphite. In the β surface model, the surface layer (rotated layer) has only one interface with bulk, and its formation energy is reduced to almost half (5.4 meV/atom). Checks performed on larger, six layer models (*AABABA* and *BABABA*) yielded 5.3 meV/atom, showing the insensitivity to deeper layers.

At first sight, the energy profile of the β bulk model (Fig. 10) clearly confirms, one more time, the discontinuity between the perfect structures at 0°/60° and the rotation structures. Rotation structures are energetically higher in the plot, clearly different from the perfect *BA*-stacked graphite, and lie in a range between 2.56 and 3.68 meV/atom. The form of relative formation energy plot versus the RRA corresponds to a parabolic function with its minimum energy at 30° RRA and its maxima at the extremes. An important conclusion can be drawn from this plot: Moiré pattern structures or rotation structures that can be visualized (only those with $0° < \mathrm{RRA} < 15°$) are the least stable structures of all, by around 1 meV/atom less stable than rotation structures that do not show Moiré patterns. The rotation structures with RRAs around 30° are the most stable structures, although these structures—as was shown above—did not conform to any visual pattern in STM. The energy profile for the α bulk model and β surface model (the rest of the data in Table I) confirm the β bulk model results and demonstrate the insensitivity of the energy profile to translation. Therefore, in interpreting STM pictures of Moiré patterns on graphite, rotational misalignments must be taken into account, whereas translational misalignments can be discarded. The β surface model confirms that bulk models overestimate the relative formation energy and it gives a more reliable energy range for the rotation structures (between 1.81 and 2.70 meV/atom less stable than perfect *BA*-stacked graphite, somewhat greater than half the bulk model values). The α bulk model reveals that the rotation structures are closer to *BA*-stacked graphite than *AA*-stacked graphite in terms of energetic stability. The extremes of the energy plots represent an energetic barrier when rotation starts from perfect *BA*-stacked graphite to Moiré structures. We suppose that the energetic barrier should not be higher than the energy difference between *AABAB*- and *BABAB*-stacked graphite, 5.4 meV/atom, nor probably it should be lower than 2.7 meV/atom (relative formation energy of the first Moiré structure with 7.34° RRA). In consequence, as this hypothetical energy barrier can become extremely high if just several hundreds of atoms are taken into account, it seems reasonable that a more flexible model is needed to explain the transitional process between perfect graphite structures and the Moiré structures with low RRAs. Actually, this last fact could support the experimental finding that Moiré structures on graphite never form huge domains but, rather, a conglomerate of small domains.

The interlayer separations do not vary broadly between the *BA*- and *AA*-stacked graphite distances—which are the minimum and maximum, respectively—but they vary in a small range close to the *BA*-stacked graphite separation: from 3.410 to 3.428 Å (see Fig. 12). However, our results do not match with Rong and Kuiper's experimental values, which were measured to be even closer to that of *BA*-stacked graphite, 3.3 Å.[10] The first interlayer separation resembles the d_{002} spacing, which is taken as a measure of turbostratic disorder. Our range of interlayer separations falls in the first stages of the interlayer spacing changes stated by Lachter and Bragg, 3.36–3.67 Å, when graphite is irradiated.[58] d_{002} changes have been interpreted in terms of a variety of defects including vacancies, interstitials, and vacancy lines and loops, but our findings suggest that, at least, at the first stages the simple mismatching of graphene layers can lead to such changes. Like the relationship between the relative formation energy and the RRA, the interlayer separation versus the RRA exhibits a parabolic function. The shortest distance is achieved in a few rotation structures around 30° RRA; this is when the relative formation energy is at its minimum and the percentages of *BA*- and *AA*-stacked graphite regions are also at their minimum. On the other hand, as RRAs become smaller, the interlayer distance lengthens steadily, the percentages of *AA*- and *BA*-stacked graphite regions expand, and the relative formation energies increase (compare Figs. 8, 10, and 12). For instance, for a decrease of 2° from 12° to 10° RRA, the Moiré pattern will show up clearer and will cause an increase of 2.5% of AA-stacked graphite, of 6.3% of *BA*-stacked graphite, of 0.002 Å in the interlayer separation, and of 0.13 meV/atom in the relative formation energy.

TABLE I. Relative formation energies and description of all computed rotation structures by models.

Relative rotation angle, RRA,[a] (deg)	n,m[b]	Number of atoms per unit cell	Periodicity of the Moiré patterns, D (Å)[c]	First interlayer separation[d] (Å)	Relative formation energy[e] (meV/atom)
		Reference structures			
BA		4		3.321	0.00
AA		2		3.591	10.25
BABA		8		3.321	0.00
AABA		8		3.591	5.36
BABABA		12		3.321	0.00
AABABA		12		3.591	5.27
		β bulk model			
6.01,53.99	6, 5	364	23.5	3.428	3.68
7.34,52.66	5, 4	244	19.2	3.424	3.43
9.43,50.57	4, 3	148	15.0	3.422	3.08
15.18,44.82	6, 1	172	9.3	3.417	2.83
16.43,43.57	5, 3	196	8.6	3.415	2.79
17.90,42.10	5,1	124	7.9	3.414	2.60
21.79,38.21	2,1	28	6.5	3.412	2.65
24.43,35.57	7, 2	268	5.8	3.411	2.72
26.01,33.99	7, 3	316	5.5	3.410	2.62
27.80,32.20	3,1	52	5.1	3.410	2.56
		α bulk model			
6.01,53.99	6,5	364	23.5	3.428	3.62
7.34,52.66	5,4	244	19.2	3.424	3.43
9.43,50.57	4,3	148	15.0	3.421	3.08
10.42,49.58	9,1	364	13.6	3.420	3.30
10.99,49.01	7,5	436	12.9	3.420	3.33
11.64,48.36	8,1	292	12.2	3.421	3.15
13.17,46.83	3,2	76	10.7	3.419	3.14
15.18,44.82	6,1	172	9.3	3.414	2.83
16.43,43.57	5,3	196	8.6	3.414	2.79
17.90,42.10	5,1	124	7.9	3.416	2.60
21.79,38.21	2,1	28	6.5	3.410	2.75
24.43,35.57	7,2	268	5.8	3.411	2.72
26.01,33.99	7,3	316	5.5	3.411	2.60
27.80,32.20	3,1	52	5.1	3.408	2.64
29.41,30.59	8,3	388	4.9	3.406	2.43
		β surface model			
7.34,52.66	5,4	488	19.2	3.424[d]	2.70
9.43,50.57	4,3	296	15.0	3.422[d]	2.22
13.17,46.83	3,2	152	10.7	3.420[d]	2.12
15.18,44.82	6,1	344	9.3	3.417[d]	2.33
16.43,43.57	5,3	392	8.6	3.415[d]	2.21
17.90,42.10	5,1	248	7.9	3.414[d]	1.98
21.79,38.21	2,1	56	6.5	3.412[d]	1.83
27.80,32.20	3,1	104	5.1	3.410[d]	1.81

[a]Both RRAs are equivalent angles due to the symmetry axis at 30°.

[b](n,m) are the components of the vector $\mathbf{V}=n\mathbf{A}+m\mathbf{B}$, where $(\mathbf{A},\mathbf{B})$ are vectors of graphene, see Fig. 2 for a scheme. RRA is the angle between the **A** vector and the **V** vector.

[c]The RRA and the periodicity of a Moiré pattern, D, are related as $D=d/[2\sin(\mathrm{RRA}/2)]$, where $d=2.452$ Å is the lattice constant of graphite.

[d]In the β surface model, the first interlayer separation of the rotated layer is taken from those calculated in the β bulk model and then the structure is allowed to relax.

[e]Relative formation energy per atom at the two topmost lyers with respect to *BA*-stacked graphite for bulk models and with respect to *BABA* for the β surface model.

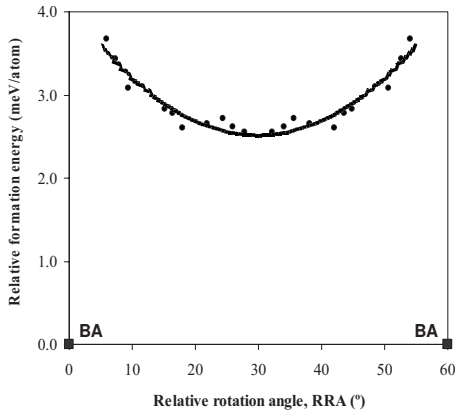

FIG. 10. Relative formation energies (RFE, meV/atom) of selected rotation structures for the β bulk model. The starting and final graphite structures show perfect *BA* stacking (0° and 60°). Notice the symmetry of the graph about 30°. Dots represent rotation structures; the dashed line is the parabolic tendency line, RFE $=1.715\times10^{-3}$ (RRA-30)^2+2.521; and finally, the squares represent the perfect *BA* graphite.

Thus, our calculations reveal quasilinear relationships between the relative formation energy, the interlayer separation, and the percentage of *AA*- and *BA*-stacked graphite. Figure 13 plots one of these relationships. To sum up, the interlayer distance is generally affected by variation of the RRA, which might be attributed to the percentage changes of the different local graphite stackings.

IV. SUMMARY

Superperiodic structures on the top graphite layers are found by means of STM spectroscopy. These superlattices are interpreted as Moiré patterns caused by a twisting of the top graphite surface layer with respect to the bulk lattice. The

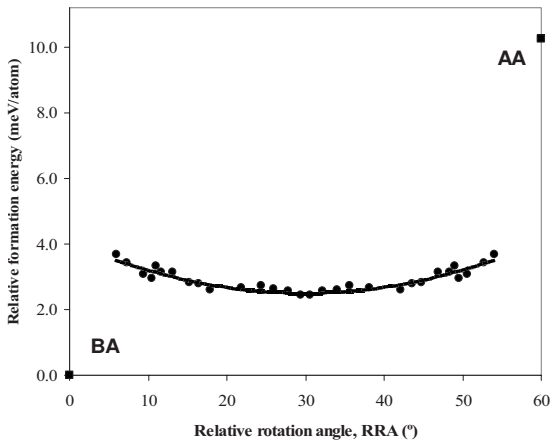

FIG. 11. RFE (meV/atom) of selected rotation structures for the α bulk model. The starting graphite structure (0°) shows perfect *BA* stacking, whereas the final one (60°) shows perfect *AA* stacking. Notice the symmetry of the graph about 30°. Dots represent rotation structures; the dashed line is the parabolic tendency line, RFE $=1.761\times10^{-3}$ (RRA-30)^2+2.515; and finally, the squares represent the values for perfect *BA* and *AA* graphites.

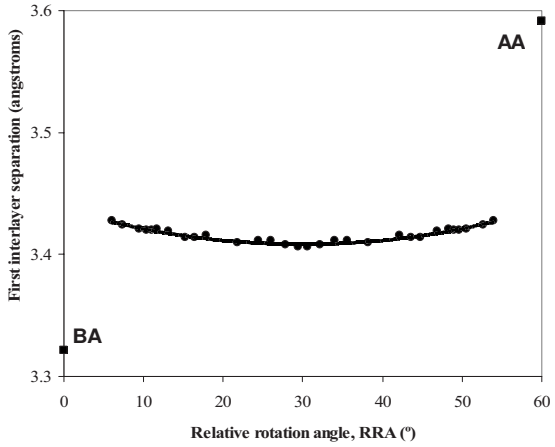

FIG. 12. First interlayer separation (FIS, Å) of selected rotation structures for the α bulk model. The starting graphite structure (0°) shows perfect *BA* stacking, whereas the final one (60°) shows perfect *AA* stacking. Notice the symmetry of the graph about 30°. Dots represent rotation structures; the dashed line is the parabolic tendency line, FIS$=3.195\times10^{-5}$ (RRA-30)^2+3.409; and finally, the squares represent the perfect *BA* and *AA* graphites.

Moiré patterns on graphite consist of huge hexagonal lattices made of bright spots. This study has unravelled some unsolved questions on Moiré patterns: (a) What is the correct correlation between local graphite stackings and the brightness of the STM images? (b) Which rotation structures exhibit Moiré patterns? (c) What is the energy profile of the rotation? and (d) Are Moiré patterns local energy minima in those profiles?

STM images map the local densities of states of a sample surface, enabling it to distinguish between α and β carbon atoms in perfect *BA*-stacked graphite. Only β carbon atoms turn out to be visible (bright areas in STM images), whereas

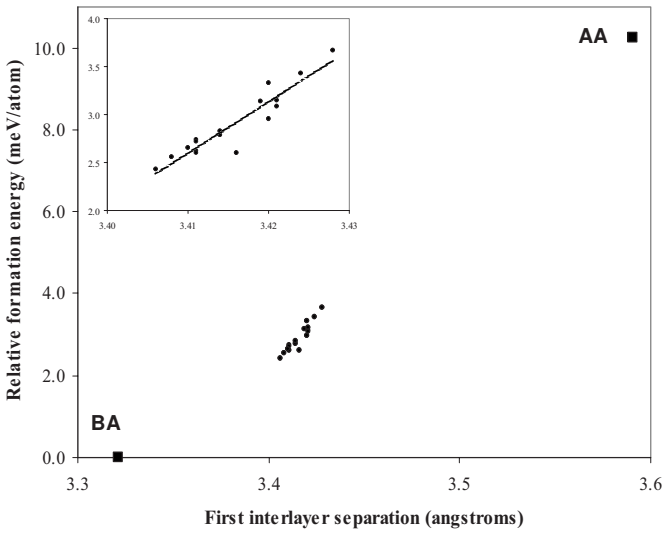

FIG. 13. Correlation between the RFE (meV/atom) and the FIS (Å) of selected rotation structures for the α bulk model. Dots represent rotation structures; the dashed line is the linear tendency line, RFE=53.598 FIS-180.17; and finally, the squares represent the perfect *BA* and *AA* graphites.

α carbon atoms remain invisible (dark areas). Analogously, Moiré structures consist of three types of regions of high rotational symmetry: *AA*-, *BA*-, and Slip*BA*-stacked graphite regions. DFT calculations on DOS at the Fermi level lead to the conclusion that only *BA*-stacked graphite regions are invisible, whereas *AA*-stacked graphite regions are the most visible, represented by bright spots, and Slip*BA*-stacked graphite regions show an intermediate brightness in the STM images. These findings reinforce and are in excellent agreement with those explained by Rong and Kuiper's model. The percentages of these three types of local graphite stackings vary drastically in the range of the relative rotation angles from 0° to 60°, leading to an assorted range of Moiré patterns with different periodicities and sizes of bright spots.

However, not all rotation structures show Moiré patterns, only under relative rotation angles between 0° and 15° (or equivalently between 45° and 60°). In the range of 15°–45°, STM images of rotation structures would yield a gray picture with no clear distinction of any kind of pattern. The breakpoint at 15° and above represents the point where the Slip*BA*-stacked graphite region becomes predominant and, consequently, the point where the *AA*-stacked graphite regions responsible for the bright spots disappear. These statements can be made regardless of the rotational center, α or β, and thus, translational movements do not affect Moiré patterns on graphite. In addition to all of that, the energy profile revealed that rotation structures with Moiré patterns were not the most stable structures. Therefore, those initially rotated structures (0°–15°) would tend to stabilize themselves to rotations around 30° under thermodynamic equilibrium. Thus, these Moiré patterns on graphite seem to be the rarest ones among the whole group of rotation structures, since the most stable rotation structures do not show any pattern and, consequently, in those cases, STM images should capture only a gray picture.

The fact that the stacked profile correlates well with the energy profile supports the idea that Moiré patterns on graphite are mainly an electronic effect rather than a real physical buckling. In addition to this correlation, there is also the correlation between the energy stability and the first interlayer separation, which ranges from 3.406 to 3.428 Å. As the relative rotation angle decreases from 15°, the Moiré pattern becomes more obvious, the first interlayer separation lengthens, the percentage of *AA*-stacked graphite increases, and the energetic stability of the structure decreases. Furthermore, the model uncovers that the energy barrier to start such a rotation needs a minimum of approximately 2.7 meV/atom, although a more sophisticated model should be built in order to verify that value and to consider the effect of rotation of small, finite domains.

ACKNOWLEDGMENTS

This work was supported by the Spanish Ministry of Education and Science (MEC) Contract No. (EX2005-0779). We also gratefully acknowledge support from British Energy Generation Ltd. The views expressed in this paper are those of the authors and do not necessarily represent the views of British Energy Generation Ltd.

*Corresponding author: FAX: +44 1273 677196; jmc23@sussex.ac.uk

[1] G. Binnig, H. Rohrer, C. Gerber, and E. Weibel, Phys. Rev. Lett. **50**, 120 (1983).

[2] A. A. El-Barbary, R. H. Telling, C. P. Ewels, M. I. Heggie, and P. R. Briddon, Phys. Rev. B **68**, 144107 (2003).

[3] K. Kobayashi, Phys. Rev. B **61**, 8496 (2000).

[4] J. T. Li, R. Berndt, and W.-D. Schneider, Appl. Phys. Lett. **67**, 921 (1995).

[5] B. An, S. Fukuyama, K. Yokogawa, M. Yoshimura, M. Egashira, Y. Korai, and I. Mochida, Appl. Phys. Lett. **78**, 3696 (2001).

[6] Q. M. Zhang, H. K. Kim, and M. H. W. Chan, Phys. Rev. B **33**, 413 (1986); P. K. Hansma, Bull. Am. Phys. Soc. **30**, 251 (1985).

[7] G. Binnig, H. Fuchs, C. Gerber, H. Rohrer, E. Stoll, and E. Tosatti, Europhys. Lett. **1**, 31 (1986).

[8] S. Park and C. F. Quate, Appl. Phys. Lett. **48**, 112 (1986); H. J. Mamin, E. Ganz, D. W. Abraham, R. E. Thomson, and J. Clarke, Phys. Rev. B **34**, 9015 (1986); H. A. Mizes and J. S. Foster, Science **244**, 559 (1989); A. Selloni, P. Carnevali, E. Tosatti, and C. D. Chen, Phys. Rev. B **31**, 2602 (1985); , Phys. Rev. B **34**, 7406 (1986); J. Tersoff, Phys. Rev. Lett. **57**, 440 (1986); I. P. Batra and S. Ciraci, J. Vac. Sci. Technol. A **6**, 313 (1988); I. P. Batra, N. Garcia, H. Rohrer, H. Salemink, E. Stoll, and S. Ciraci, Surf. Sci. **181**, 126 (1987); J. M. Soler, A. M. Baro, N. Garcia, and H. Rohrer, Phys. Rev. Lett. **57**, 444 (1986); M. Salmeron, D. F. Ogletree, C. Ocal, H. C. Wang, G. Neubauer, W. Kolbe, and G. Meyers, J. Vac. Sci. Technol. B **9**, 1347 (1991).

[9] H. Chang and A. J. Bard, Langmuir **7**, 1143 (1991); V. J. Cee, D. L. Patrick, and T. P. Beebe, Jr., Surf. Sci. **329**, 141 (1994); J. E. Buckley, J. L. Wragg, and H. W. White, J. Vac. Sci. Technol. B **9**, 1079 (1991); X. Yang, Ch. Bromm, U. Geyer, and G. von Minnigerode, Ann. Phys. (Leipzig) **1**, 3 (1992).

[10] Z. Y. Rong and P. Kuiper, Phys. Rev. B **48**, 17427 (1993).

[11] T. A. Land, T. Michely, R. J. Behm, J. C. Hemminger, and G. Comsa, Surf. Sci. **264**, 261 (1992).

[12] V. Elings, and F. Wudl, J. Vac. Sci. Technol. A **6**, 412 (1987); J. Osing and I. V. Shvets, Surf. Sci. **417**, 145 (1998); H. Beyer, M. Muller, and P. J. Ouseph, Appl. Surf. Sci. **165**, 38 (2000); J. W. Lyding, J. S. Hubacek, G. Gammie, S. Skala, R. Brockenbrough, J. R. Shapley, and M. P. Keyes, J. Vac. Sci. Technol. A **6**, 363 (1988); T. M. Bernhardt, B. Kaiser, and K. Rademann, Surf. Sci. **408**, 86 (1998); H. L. Sun, Q. T. Shen, J. F. Jia, Q. Z. Zhang, and Q. K. Xue, *ibid.* **542**, 94 (2003).

[13] V. J. Cee, D. L. Patrick, and T. P. Beebe. Jr., Surf. Sci. **329**, 141 (1995).

[14] P. I. Oden, T. Thundat, L. A. Nagahara, S. M. Lindsay, G. B. Adams, and O. F. Sankey, Surf. Sci. **181**, 126 (1987).

[15] Z. Y. Rong, Phys. Rev. B **50**, 1839 (1994).

[16] H. Beyer, M. Muller, and T. H. Schimmel, Appl. Phys. A: Mater. Sci. Process. **68**, 163 (1999).

[17] M. Sasaki, Y. Yamada, Y. Ogiwara, S. Yagyu, and S. Yamamoto, Phys. Rev. B **61**, 15653 (2000); M. Enachescu, D. Schleef, D. F. Ogletree, and M. Salmeron, *ibid.* **60**, 16913 (1999).
[18] D.-Q. Yang, G.-X. Zhang, and E. Sacher, J. Phys. Chem. B **110**, 8348 (2006).
[19] Y. Gan, W. Chu, and L. Qiao, Surf. Sci. **539**, 120 (2003); T. R. Albrecht, H. A. Mizes, J. Nogami, Sang-il Park, and C. F. Quate, Appl. Phys. Lett. **52**, 362 (1988); P. Simonis, C. Goffaux, P. A. Thiry, L. P. Biro, Ph. Lambin, and V. Meunier, Surf. Sci. **511**, 319 (2002).
[20] G. G. Wildgoose, M. E. Hyde, N. S. Lawrence, H. C. Leventis, T. G. J. Jones, and R. G. Compton, Langmuir **21**, 4584 (2005).
[21] Y. Baskin and L. Meyer, Phys. Rev. **100**, 544 (1955).
[22] M. Kuwabara, D. R. Clarke, and D. A. Smith, Appl. Phys. Lett. **56**, 2396 (1990).
[23] J. Xhie, K. Sattler, M. Ge, and N. Venkateswaran, Phys. Rev. B **47**, 15835 (1993).
[24] R. Wiesendanger, *Scanning Tunneling Microscopy and Spectroscopy: Methods and Applications* (Cambridge University Press, Cambridge, 1994); R. C. Tatar and S. Rabii, Phys. Rev. B **25**, 4126 (1982).
[25] D. Tománek, S. G. Louie, H. J. Mamin, D. W. Abraham, R. E. Thomson, E. Ganz, and J. Clarke, Phys. Rev. B **35**, 7790 (1987).
[26] J. Schneir, R. Sonnenfeld, P. K. Hansma, and J. Tersoff, Phys. Rev. B **34**, 4979 (1986).
[27] A. L. Tchougreeff, J. Phys. Chem. **100**, 14048 (1996).
[28] Y. Wang, Y. Ye, and K. Wu, Surf. Sci. **600**, 729 (2006).
[29] P. Moriarty and G. Hughes, Appl. Phys. Lett. **60**, 2338 (1992); P. J. Ouseph, T. Poothackanal, and G. Mathew, Phys. Lett. A **205**, 65 (1995); J. I. Paredes, A. M. Alonso, and J. M. D. Tascon, Carbon **39**, 473 (2001); D. Tomanek and S. G. Louie, Phys. Rev. B **37**, 8327 (1988).
[30] Wing-Tat Pong and Colm Durkan, J. Phys. D **38**, R329 (2005).
[31] P. R. Briddon and R. Jones, Phys. Status Solidi B **217**, 131 (2000).
[32] J. P. Perdew and Y. Wang, Phys. Rev. B **45**, 13244 (1992).
[33] C. Hartwigsen, S. Goedecker, and J. Hutter, Phys. Rev. B **58**, 3641 (1998).
[34] H. J. Monkhorst and J. D. Pack, Phys. Rev. B **13**, 5188 (1976).
[35] Y. C. Wang, K. Scheerschmidt, and U. Gosele, Phys. Rev. B **61**, 12864 (2000).
[36] S. P. Kelty and C. M. Lieber, J. Phys. Chem. **93**, 5983 (1989); Phys. Rev. B **40**, 5856 (1989).
[37] P. J. Ouseph, Phys. Rev. B **53**, 9610 (1996).
[38] J. Garbarz, E. Lacaze, G. Faivre, S. Gauthier, and M. Schott, Philos. Mag. A **65**, 853 (1992).
[39] C.-Y. Liu, H. Chang, and A. J. Bard, Langmuir **7**, 1138 (1991).
[40] These results are in line with those published by J.-C. Charlier, J.-P. Michenaud, and Ph. Lambin, Phys. Rev. B **46**, 4540 (1993). The LDOS at the Fermi level for *AA*-, *BA*-, and *CAB*-stacked graphite are reported to be 0.0085, 0.0033, and 0.0021 states/eV atom, respectively. Through our calculations, we found 0.0082 states/eV atom for *AA*-stacked graphite and 0.0040 states/eV atom for *BA*-stacked graphite.
[41] Notice that our calculations predict that *BABABAB* would be the darkest area and *CBAABAB* the second darkest, although the difference in the LDOS is really small. Meanwhile, in Rong and Kuiper's model, that relation is reversed.
[42] J. H. Wu, F. Hagelberg, and K. Sattler, Phys. Rev. B **72**, 085441 (2005).
[43] B. T. Kelly, *Physics of Graphite* (Applied Science, London, 1981).
[44] It needs to be said that, for the α bulk model, this simplification is just a good approximation, since this model is not fully symmetric around 30° rotation. However, it should only show a weak shift from it.
[45] J. Tersoff and D. R. Hamann, Phys. Rev. Lett. **50**, 1998 (1983); , Phys. Rev. B **31**, 805 (1985).
[46] S. Ranganathan, Acta Crystallogr. **21**, 197 (1966).
[47] H. Beyer, M. Muller, and Th. Schimmel, Appl. Phys. A: Mater. Sci. Process. **68**, 163 (1999); H. L. Sun, Q. T. Shen, J. F. Jia, Q. Z. Zhang, and Q. K. Xue, Surf. Sci. **542**, 94 (2003).
[48] J. W. G. Wildöer, L. C. Venema, A. G. Rinzler, R. E. Smalley, and C. Dekker, Nature (London) **391**, 59 (1998); T. W. Odom, J.-L. Huang, P. Kim, and C. M. Lieber, *ibid.* **391**, 62 (1998).
[49] V. Meunier and Ph. Lambin, Phys. Rev. Lett. **81**, 5588 (1998).
[50] Note that the RRA was miscalculated in Ref. 28. The RRA is calculated from the experimentally measured periodicity (D) using the formula $D=d/[2\sin(\mathrm{RRA}/2)]$, where $d=2.452$ Å. For $D=110$ Å, it results in RRA=1.28° instead of 2.56° stated by Ref. 28.
[51] Unit cells with less than 500 atoms have been left out of the calculations because the algorithm gives unreliable values for this kind of structure.
[52] When Slip*BA* is dominant, the stacking usually tends to random (i.e., turbostatic) rather than forming a regular stacking. The Slip*BA* local stacking is properly found in coexistence with *AA*- and *BA*-stacked graphite regions.
[53] J. C. Charlier, X. Gonze, and J. P. Michenaud, Europhys. Lett. **28**, 403 (1994).
[54] G. Sun, M. Kertesz, J. Kurti, and R. H. Baughman, Phys. Rev. B **68**, 125411 (2003); S. D. Chakarova and E. Schroder, J. Chem. Phys. **122**, 054102 (2005).
[55] Then the six points were fitted to a second order polynomial to find the distance that minimizes the energy.
[56] M. S. Dresselhaus and G. Dresselhaus, Adv. Phys. **51**, 1 (2002).
[57] M. K. Song, S. D. Hong, and K. T. No, J. Electrochem. Soc. **148**, A1159 (2001); A. N. Kolmogorov and V. H. Crespi, Phys. Rev. Lett. **85**, 4727 (2000).
[58] J. Lachter and R. H. Bragg, Phys. Rev. B **33**, 8903 (1986).